ELSEVIER

Chemical Geology 236 (2007) 303–322

CHEMICAL GEOLOGY
INCLUDING
ISOTOPE GEOSCIENCE

www.elsevier.com/locate/chemgeo

Determination of sulfur speciation and oxidation state of olivine hosted melt inclusions

Michael C. Rowe [a,b,*], Adam J.R. Kent [a], Roger L. Nielsen [a]

[a] Department of Geosciences, Oregon State University, Corvallis, OR 97331, USA
[b] Department of Geological Sciences, University of Texas at Austin, Austin, TX 78712, USA

Received 27 March 2006; received in revised form 9 October 2006; accepted 13 October 2006

Editor: R.L. Rudnick

Abstract

In order to better understand what controls sulfur speciation in melt inclusions, and how that pertains to the original basalt composition, we have conducted a series of heating experiments on naturally quenched and crystalline olivine-hosted melt inclusions. Sulfur speciation was determined from S Kα peak shift measurements by electron microprobe on the experimentally heated inclusions as well as a series of naturally quenched inclusions, and matrix glasses.

Naturally quenched olivine-hosted melt inclusions record a similar but more variable sulfur speciation relative to matrix glasses, (up to 45–50% variation in S^{6+}/S_{total}). Much of this range can be attributed to the effect of degassing which may either increase or decrease the S^{6+}/S_{total}. In addition, olivine melt re equilibration and H diffusion out of the inclusion both potentially result in the oxidation of melt inclusions. Heating of melt inclusions can have different effects on the sulfur speciation under different conditions. A slight decrease in S^{6+}/S_{total} and oxygen fugacity (~0.1 log units) can occur from overheating of inclusions (above the temperature of entrapment), resulting from excess ferrous iron in the melt. An increase in heating times should result in an oxidation of the inclusion generated by increased H diffusion out of the inclusion. However, results of heating experiments on melt inclusions from an Izu backarc basalt for less than 30 min do not show a significant increase in sulfur oxidation. In addition, experiments conducted at both IW and FMQ have measured sulfur speciation consistent with naturally quenched inclusions suggesting that at experimental temperatures near that of olivine crystallization the furnace atmosphere does not exert significant control on the melt fO_2. By taking these parameters into account, sulfur speciation and oxidation state of basaltic melt trapped within inclusions can be accurately determined from both naturally quenched and heated olivine hosted melt inclusions.

Keywords: Sulfur speciation; Melt inclusions; Experimental petrology; Oxidation state; Electron microprobe

1. Introduction

An accurate and precise determination of sulfur speciation can provide constraints on the sulfur solubility and oxidation state of magmas. As a dissolved species in magmas, sulfur dominantly exists as sulfide (S^{2-}) under reducing conditions, below the Fayalite–Magnetite–Quartz (FMQ) oxygen buffer, and sulfate (S^{6+}) under oxidizing conditions (>FMQ+2 log units; Carroll and Rutherford, 1988; Wallace and Carmichael, 1992). Recent work has also indicated that several other species including sulfite (S^{4+}) and other radical anions

* Corresponding author. Department of Geological Sciences, University of Texas at Austin, Austin, TX 78712, USA. Tel.: +1 512 471 8054.
E-mail address: rowem@mail.utexas.edu (M.C. Rowe).

0009-2541/$ - see front matter © 2006 Elsevier B.V. All rights reserved.
doi:10.1016/j.chemgeo.2006.10.007

(S_2^-, S_3^-) may also be present in significant concentrations and that sulfite may be influential at oxidation states between FMQ and FMQ+2 (Metrich et al., 2002; Winther et al., 1998; Jugo et al., 2005a). Less is known, however, about the solubility and relative proportions of these other species in magmas. Sulfur solubility is strongly dependant on speciation and oxidation state, with nearly 10 times greater sulfur concentrations in basaltic magmas at high fO_2 and S^{6+}/S_{total} (Jugo et al., 2005b). The dependence of solubility on speciation therefore has significant implications for numerous igneous processes and is especially relevant for volatile budgets and fluxes in subduction zones, volcanic degassing and ore genesis (for example: Luhr, 1990; Imai et al., 1993; Hedenquist and Lowenstern, 1994; Wallace, 2003; De Hoog et al., 2004; Wallace, 2005).

Magmatic oxidation states, and therefore sulfur speciation can also be strongly influenced by processes such as assimilation, fractional crystallization, and degassing (Mathez, 1984; Carmichael and Ghiorso, 1986, 1990; Sato and Wright, 1966). Melt inclusions trapped within early crystallizing phases provide a means of preserving melt compositions prior to significant modification of the magma. Analysis of these inclusions may provide better constraints on the oxidation state of the magma prior to significant assimilation, crystallization and degassing.

Electron microprobe determination of the relative proportions of sulfide (S^{2-}) and sulfate (S^{6+}) is based on the position of the sulfur Kα X-ray peak (Fig. 1; Carroll and Rutherford, 1988; Wallace and Carmichael, 1994; Matthews et al., 1999; Jugo et al., 2005a). This technique provides relatively rapid analysis (50–100 min/sample) of small samples (~30 μm) and is therefore ideal for application to melt inclusions. However, olivine-hosted melt inclusions provide additional complications due to the potential for post-entrapment modification of the oxidation state through re-equilibration with the host, fractional crystallization or melting, and H diffusion out of the melt inclusion and olivine (Cottrell et al., 2002; Hauri, 2002; Danyushevsky et al., 2000, 2002). In addition, melt inclusions from slowly cooled lavas often require rehomogenization due to the growth of daughter crystals within the inclusions and host mineral growth on the inclusion-host interface (Roedder, 1979; Nielsen et al., 1998; Danyushevsky et al., 2002). Rehomogenization is the process of heating inclusions to temperatures near that of melt entrapment (or olivine crystallization), resulting in the melting of microlites and host-mineral growth along the inclusion-mineral interface, thus producing a melt composition similar to that of the initially trapped melt inclusions (See Danyushevsky et al., 2002 for a detailed discussion of melt inclusion rehomogenization). However, little is known about the effects of heating on oxidation states of melt inclusions (for example: Danyushevsky et al., 2002). One possible consequence of heating melt inclusions is that the melting of the host olivine may cause a reduction in the melt oxidation state due to the increase in ferrous iron. In addition to dehydration of melt inclusions and increasing homogenization temperatures, long heating times of homogenization may also result in the diffusion of H from the melt inclusion, causing oxidation of the melt (Hauri, 2002; Danyushevsky et al., 2002; Massare et al., 2002). The presence of sulfide globules in melt inclusions, forming either from H diffusion out of the inclusions or from Fe-loss during olivine-inclusion re-equilibration, may result in a lower sulfur concentration and increased relative proportion of sulfate in the inclusions (Metrich et al., 1999; Danyushevsky et al., 2002).

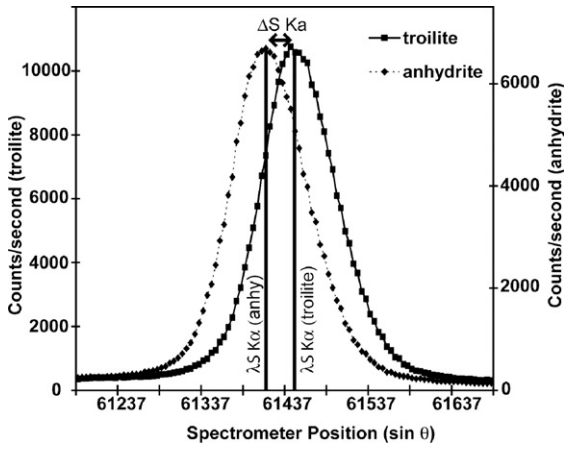

Fig. 1. Wave scans of the SKα peak position for troilite and anhydrite standards. ΔS Kα shown here is the maximum possible shift (~3.0 Å*10^3) between sulfate (S^{6+}) and sulfide (S^{2-}).

This study addresses several analytical, experimental, and natural problems related to the determination of oxidation states and sulfur speciation in olivine-hosted melt inclusions. Through use of both naturally glassy melt inclusions and experimentally heated melt inclusions, we investigate the effects of H diffusion, magmatic degassing, olivine-melt re-equilibration, fractional crystallization and melting, and rehomogenization on melt sulfur speciation and oxidation state in basaltic melts. We show that with careful analysis and sample selection this technique provides reliable information on the sulfur speciation and oxidation state of the originally trapped melt.

2. Sample description

Four olivine-bearing basalts were selected for this study, two Oregon Cascade basalts, one Loihi pillow basalt, and one Izu backarc basalt.

2.1. Loihi pillow basalt (LO-02-02; LO-02-04)

Loihi pillow lava samples LO-02-02 and LO-02-04 were collected by dredge 2 at a depth of 4200 m during the 1989 Tunes IV expedition of the R/V Thomas Washington. Samples were dredged from the southern rift zone of Loihi seamount (18.77° N; 155.18° W; Kent et al., 1999a). LO-02-02 and LO-02-04 have similar modal mineralogy, glass inclusion and groundmass compositions and may be samples of the same flow (Kent et al., 1999a). Naturally quenched, olivine-hosted glassy melt inclusions range from 9.71–11.57 wt.% MgO as opposed to ~9 wt.% MgO for the matrix glass. Reported olivine compositions range from $Fo_{86.0}$ to $Fo_{87.8}$ in LO-02-02.

Prior studies of Loihi basalt LO-02-02 and LO-02-04 (Kent et al., 1999a,b) have presented evidence of significant assimilation of a seawater derived component resulting in matrix glass with major element compositions similar to those observed in melt inclusions but with high H_2O (1.6 wt.%) and Cl (0.14 wt.%). The variability of melt inclusion compositions (0.031–0.095 wt.% Cl; 0.59–1.67 wt.% H_2O) reported by Kent et al. (1999a,b) have been interpreted to represent the range of melts in the Loihi magmatic system prior to their aggregating and homogenizing in the magmatic conduit system.

Naturally glassy melt inclusions from LO-02-02, heated at 1200 °C (at FMQ) for 15 min and 30 min, have been previously analyzed for water loss during heating experiments (A.J.R. Kent, unpublished data). Water contents range from 1.0–1.4 wt.% in inclusions heated for 15 min compared to 0.6–0.7 wt.% H_2O measured in inclusions heated for 30 min (Table 2). Water concentrations for unheated inclusions reported in Table 2 are unknown. Reanalyzing these melt inclusions for sulfur speciation allows us to 1) examine possible changes in the sulfur speciation as a function of heating time and 2) directly compare sulfur speciation and oxidation state with magmatic water content.

2.2. Izu backarc basalt (31-7B)

Sample 31-7B is a submarine basalt collected from a backarc knoll in the Izu arc (latitude 30.69° N; longitude 140.02° E). The basalt sample was collected during dredge 31 by J. Gill and A. Hochstaedter (Hochstaedter et al., 2000). Major element concentrations from bulk rock analysis indicate that 31-7B is a low K_2O (0.33 wt.%; 2.89 wt.% total alkalies) basalt with 7.20 wt.% MgO and 9.39 wt.% FeO* (J. Gill and D. Tollstrup, unpublished data). Olivine is the dominant phenocryst phase with lesser proportions of plagioclase and clinopyroxene. Olivine compositions range from $Fo_{80.5}$ to $Fo_{85.1}$ (mean of $Fo_{82.3}$).

2.3. Quartzville basalt (QV04-3B)

A sample from a young cinder cone in the Quartzville mining district in the western Oregon Cascades was used in order to expand the compositional range of the systems we examined. The sample is absarokitic, with high total alkalis (5.99 wt.% Na_2O+K_2O), 9.86 wt.% MgO and 6.53 wt.% FeO*. The phenocryst assemblage is olivine ($Fo_{86.1–90.5}$) with minor clinopyroxene. Previous work on this basalt has indicated that it is oxidized (NNO+1; Rowe et al., 2006) relative to other contemporary basaltic lavas in the region. Sulfur concentrations in naturally quenched melt inclusions range from 2700 ppm to 5900 ppm. In addition, sufficient sulfur was retained in the scoria glass to allow for direct comparisons of sulfur speciation between naturally quenched melt inclusions and scoria glass from the subaerial eruption.

2.4. Cayuse crater basalt (CC02-1)

Cayuse crater basalt flow, located in the Central Oregon High Cascades is a primitive calc-alkaline basalt (51.94 wt.% SiO_2, 8.62 wt.% MgO). Olivine is the only phenocryst phase present with plagioclase laths evident in the groundmass. Olivine phenocrysts have a compositional range of $Fo_{83.7}$ to $Fo_{88.3}$. Melt inclusions within this subaerially erupted lava range from mostly glassy (>90% glass) to near completely crystalline. Due to an abundance of large melt inclusions with relatively constant major-element composition, this sample provided a good case for testing the affects of rehomogenization on a subaerially erupted basalt.

3. Methods

3.1. Heating experiments and analysis

Handpicked olivines were examined in ethanol to identify melt inclusion-bearing grains. Melt inclusions were heated/rehomogenized in a 1 atm Deltech vertical quench furnace. For heating experiments in this study

we distinguish between samples which contain already glassy melt inclusions (referred to as heated), while melt inclusions which were crystalline prior to heating are referred to as rehomogenized.

A CO_2–H_2 mixture was utilized to regulate furnace atmosphere. Oxygen fugacity was maintained just below FMQ oxygen buffer for most runs, in order to inhibit magnetite crystallization (exception: one run of 31-7b olivines heated for 10 min at the IW oxygen buffer; Table 1). Except where specifically stated, experimental heating times have been kept to less than 15 min at temperatures above 1000 °C, and only 10 min at maximum temperature, to reduce H diffusion in water-bearing melt inclusions (Hauri, 2002; Danyushevsky et al., 2002). Following the heating, olivine grains were mounted in 1 in. epoxy rounds, or for small volume samples individually mounted, then polished and carbon-coated for microprobe analysis.

Glass inclusions, groundmass, and olivine grains were analyzed by electron microprobe on a Cameca SX100 at Oregon State University for major elements (and S and Cl for the glasses). Inclusions used in this study have a minimum diameter of 30 μm due to size limitations of the sulfur Kα peak shift technique. Melt inclusions were analyzed using a 7 μm, 30 nA beam with a 15 KeV accelerating voltage. A Makaopuhi Lava Lake basaltic glass (USNM 113498/1 VG-A99) was analyzed as an internal calibration standard while BCR-2G and LO-02-04 glasses were analyzed as secondary standards prior to each analytical session. Sulfur concentrations were measured near the sulfide peak position (chalcopyrite in-house standard), counting for 30 s on the peak. It should be noted that sulfur concentrations reported by Kent et al. (1999a) for LO-02-04 (700 ppm) are significantly lower then the average value of multiple analyses performed at Oregon State University on a Cameca SX50 and Cameca SX100, which yielded sulfur concentrations of ~1400 ppm. Sulfur concentrations reported by Kent et al. (1999a) however are considered unreliable (A. Kent personal communication). Olivine grains were analyzed for major elements by electron microprobe using a 50 nA, 1 μm beam with a 15 KeV accelerating voltage. Springwater meteorite olivine (USNM 2566), was analyzed prior to each analytical session as an internal standard.

Table 1
Summary of heating experiments

Sample ID	Heating time (min)	Temperature (°C)	MI (#)
31-7b	10	1143	3
31-7b[a]	10	1133	3
31-7b	20	1143	3
31-7b	30	1143	3
31-7b	10	1177	3
31-7b	10	1206	3
31-7b	10	1231	1
LO-02-02[b]	15	1200	3
LO-02-02[b]	30	1200	3
QV04-3b	10	1112–1119	2
CC02-1	15	1218–1224	6

Notes: [a]Rehomogenization conducted at the IW oxygen buffer (all other experiments at the FMQ oxygen buffer). [b]Rehomogenization performed by A.J.R. Kent (upd).

3.2. SKα X-ray wavelength shifts

The SKα wavelength (λ[Skα]) shift analyses were conducted following the methods of Wallace and Carmichael (1994) and Carroll and Rutherford (1988). Analyses were performed at Oregon State University on a Cameca SX100 electron microprobe and at the University of Oregon on a Cameca SX50 electron microprobe. SKα shifts were measured simultaneously on three PET crystals to determine the reproducibility of the measurements. Anhydrite and pyrite were analyzed at the beginning of the analytical session and pyrrhotite and/or troilite was analyzed before and after every melt inclusion to correct for instrument drift. Beam conditions for sulfur peak shift measurements were similar to that used for glass major-element analysis with a 30 nA beam current, a 15 KeV accelerating voltage, and a 5–7 μm beam diameter. Each spectrometer was moved 0.00005 sin θ units for 100 steps with a 5 s counting time for standards and 30 s counting time ([S] > 900 ppm) and 60 s counting time ([S] < 900 ppm) for glasses at each step. Each wavelength scan was fitted with a Gaussian curve to determine the peak position of the scan, reported as λ(SKα). Wavelength shifts (ΔSKα) are reported relative to troilite (FeS) in units of angstroms times 1000 (reported as $Å * 10^3$):

$$\Delta(\mathrm{SK}\alpha)_{\mathrm{Unknown}} = \lambda(\mathrm{SK}\alpha)_{\mathrm{FeS}} - \lambda(\mathrm{SK}\alpha)_{\mathrm{Unknown}} \quad (1)$$

Several additional calculations are required to determine sulfur speciation (S^{6+}/S_{total}) and magmatic oxidation state (fO_2). Sulfur speciation is calculated relative to the peak shift of anhydrite, (assumed all S^{6+}), based on the following equation (Carroll and Rutherford, 1988).

$$S^{6+}/S_{\mathrm{total}} = (\Delta(\mathrm{SK}\alpha)_{\mathrm{Unknown}}/\Delta(\mathrm{SK}\alpha)_{\mathrm{Anhydrite}}) * 100 \quad (2)$$

Wallace and Carmichael (1994) derived the following relationship to determine oxygen fugacity based on sulfur speciation:

$$\log\left(\frac{X_{S^{6+}}}{X_{S^{2-}}}\right) = a^{*}\log fO_2 + b/T(\mathrm{K}) + c \quad (3)$$

Where $a=1.02$, $b=25410$, and $c=-10$

Which when rearranged, solved for mole fraction sulfate, and referenced to the FMQ oxygen buffer (Jugo et al., 2005a) is:

$$X_{S^{6+}} = \frac{1}{[1+e^{(2.73-2.35\Delta FMQ)}]} \quad (4)$$

Where $X(S^{6+})$ is the mole fraction of sulfate.

It should be noted that Eqs. (2) (3) and (4) are based on the assumption that $S^{6+}$and $S^{2-}$are the only valence states of sulfur present. XANES sulfur K-edge analyses have identified up to 16% sulfite (S^{4+}) as a component in oxidized magmatic glasses and sulfite has been shown to co-exist with sulfate in highly oxidized Fe-free glasses (Metrich et al., 2002, 2005). However, independent experiments on sulfur speciation at high fO_2 (+5 to +6 log units ΔFMQ) indicate only the presence of sulfide and sulfate (Paris et al., 2001). Strictly speaking, when sulfite is presumed to be present, Eq. (2) should be referred to as a percent sulfate equivalent or mole fraction sulfate equivalent ($X[S^{6+}]$) after Winther et al. (1998) and Jugo et al. (2005a). However, because we have no constraints on the relative proportion of sulfite, we hold with the more commonly used notation of S^{6+}/S_{total} as representing the relative proportion of sulfate in glass.

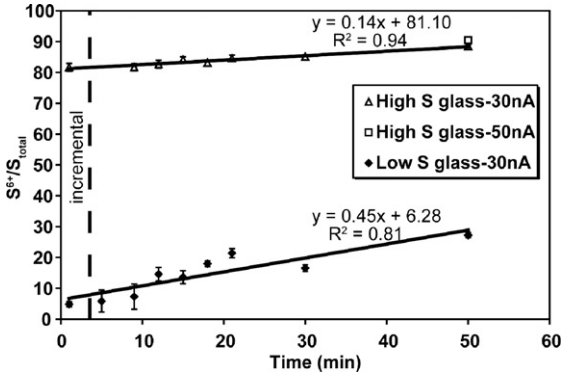

Fig. 2. Increase in S^{6+}/S_{total} with increased beam exposure time for a high sulfur glass (2700 ppm; QV04-3B) and low sulfur glass (1600 ppm; K 14-3). One minute analyses were moved incrementally at a rate of 1 μm/minute for 50 min, longer time analyses were made with a stationary beam. Error bars on individual points are the average of the three spectrometer measurements (1σ).

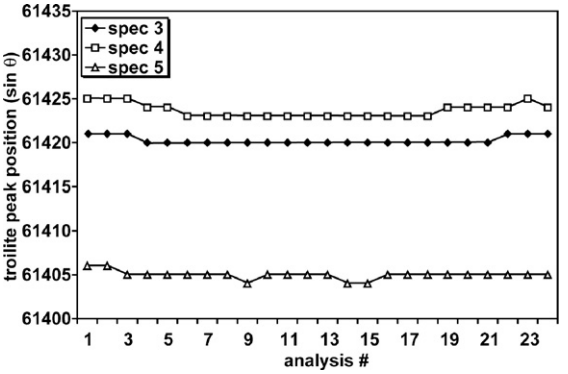

Fig. 3. Peak positions determined for 24 analyses of the troilite standard over a 24 h period for the three spectrometers. Peak positions calculated following the method described in the text. Error bars for the Gaussian peak fit (1σ) are smaller than the symbol size.

Previous sulfur peak shift studies have observed that oxidation of the sulfur, or the generation of sulfite (in water bearing glasses), in glass may occur with prolonged microbeam exposure (Wallace and Carmichael, 1994; Metrich et al., in preparation). We conducted sulfur peak shift measurements on a number of samples and standards for varying times to test whether we could reproduce this result, and create a correction for this phenomenon. In glasses it was observed that higher sulfur glasses (higher initial sulfate proportion) generally experienced less oxidation than lower sulfur glasses (Fig. 2). However, a time series analysis of troilite, anhydrite, and barite mineral standards suggest that sulfur concentration and initial oxidation state may not be the only factor in determining the magnitude of the peak shift as no peak shift was observed during long beam exposure for troilite or barite standards while a significant shift was observed for long times on the anhydrite standard. This may suggest that bond type and strength is also a factor influencing the sulfur oxidation resulting from beam exposure. Na^{+} migration has been suggested as a cause of surface oxidation of glasses (Fialin et al., 2004), however, the low S glass (Fig. 2) experiences a greater oxidation with prolonged beam time despite a lower Na_2O wt.%. To avoid an apparent increase in λ(SKα) from exposure to the electron beam, the beam location is moved incrementally at a rate of 1 μm/min. This requires there to be ~50 μm^2 of "fresh" glass to allow for complete analysis. Care was taken to avoid microprobe beam damaged spots from major element measurements.

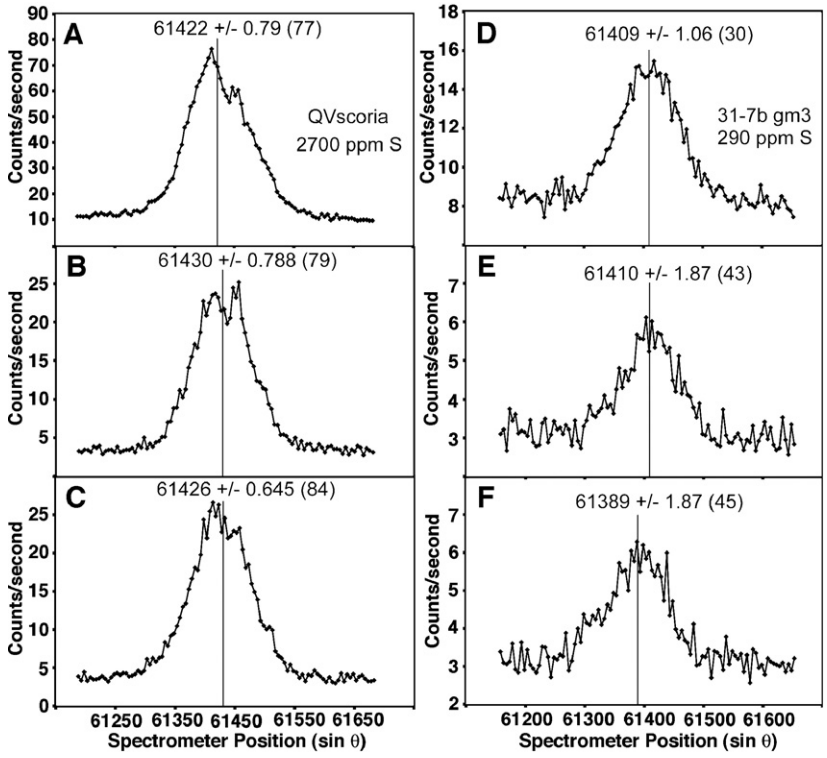

Fig. 4. Wavescan spectra for sulfur peaks from (A–C) high sulfur (QVscoria; 2700 ppm S) and (D–F) low sulfur (31-7b gm3; 290 ppm S) glasses. (A–C) Spectra are simultaneously collected on three different spectrometers with 30 s/step counting times. (D–F) Spectra are simultaneously collected based on a 60 s/step count time. Peak position and error (1σ) are determined using IgorPro software (www.wavemetrics.com). Calculated sulfate proportions are given in parentheses.

Over the course of a 24 h analytical session on the Cameca SX100 at Oregon State University, 24 troilite standard analyses were conducted (Fig. 3) to test the reproducibility of the sulfide peak position. The reproducibility of the peak position was 0.08 $Å * 10^3$ for two spectrometers and 0.12 $Å * 10^3$ for the third spectrometer (reported to 2σ). To determine reproducibility of sulfur speciation measurements we ran 6 repeat analyses of Galapagos Spreading Center (95.5° W) glass K 14-3 with the glass protocol of 30 s/step (Christie et al., 1986). The standard deviation (1σ) of the six repeat analyses was ±3.5% sulfate. Additionally, calculating oxygen fugacity following the protocol above, based on an average sulfate proportion of 1% for K 14-3 provides an fO_2 of −0.79 log units ΔFMQ, similar to the reported value of −0.74 log units ΔFMQ reported by Christie et al. (1986). Propagation of error (1σ) associated with the peak fit of a single spectrometer wave scan, and the standard deviation (1σ) of the three spectrometer measurements per analysis, are roughly equivalent to the error estimated by repeat analysis of K 14-3 glass. The peak fitting error is largely dependant on sulfur concentration of the melt inclusion and peak shape, generally increasing with decreasing sulfur content (Fig. 4).

4. Results

A total of 45 melt inclusions (12 naturally quenched, 33 heated) were analyzed for major elements (including S and Cl) and sulfur speciation by electron microprobe (Table 2). Degassing of melt inclusions occurs during heating experiments in any inclusion not isolated within its host olivine. If defects (fractures) in the host around the inclusion are present or if the inclusion is not completely enclosed, volatiles will degas at experimental temperatures. Care was taken in selection of melt inclusions for analysis to avoid inclusions which had obvious fractures which may have remained open to the magmatic system prior to initial entrapment. In addition, sulfur concentrations were monitored in melt inclusions to determine if inclusions have degassed either naturally or during rehomogenization (Nielsen et al., 1998). Typically, heated inclusions which have sulfur concentrations significantly below the Fe-sulfide saturation

Table 2
Major element and sulfur speciation analyses of melt inclusions and matrix glass

Locality	Izu backarc															
Sample	31-7B															
ID	gm.3	25a	28a	1	15	26	10-3-1	10-4-1b	10-6-1	IW-4-2[e]	IW-6-1[e]	IW-1-1[e]	20-1-2b	20-3-1	20-6-1	30-2-1a
Temperature (°C)	Matrix	Unheated	Unheated	Unheated	Unheated	Unheated	1143	1143	1143	1133	1133	1133	1143	1143	1143	1143
Time (min)							10	10	10	10	10	10	20	20	20	30
Measured melt inclusion compositions																
SiO_2	52.04	49.40	49.78	50.43	49.08	49.33	48.34	49.49	48.49	49.45	48.04	49.05	48.10	48.45	47.88	49.02
TiO_2	1.65	1.27	1.40	1.50	1.19	1.23	1.12	1.29	1.12	1.31	1.13	1.42	1.27	1.04	1.09	1.23
Al_2O_3	15.52	16.93	17.21	16.25	18.47	18.23	16.68	16.18	17.33	16.67	17.92	17.45	15.68	17.62	17.25	16.05
FeO[a]	11.34	10.24	10.05	10.51	9.40	9.22	9.65	10.70	8.64	10.40	8.55	9.72	11.99	9.04	8.99	9.80
MnO	0.19	0.18	0.16	0.17	0.16	0.14	0.17	0.17	0.19	0.18	0.18	0.18	0.23	0.16	0.17	0.17
MgO	5.64	6.18	5.54	5.29	6.28	5.66	7.53	7.22	7.64	6.87	6.82	7.29	6.88	7.64	7.75	7.51
CaO	10.50	11.53	11.29	11.68	12.11	12.25	11.61	10.50	11.61	11.07	11.82	10.98	11.07	11.65	11.61	10.69
Na_2O	3.17	2.56	2.65	2.44	2.55	2.41	2.42	2.65	2.41	2.64	2.94	2.62	2.53	2.41	2.40	2.49
K_2O	0.42	0.31	0.34	0.34	0.28	0.27	0.28	0.34	0.27	0.33	0.29	0.30	0.32	0.29	0.26	0.31
P_2O_5	0.23	0.23	0.21	0.22	0.18	0.20	0.23	0.19	0.17	0.20	0.19	0.25	0.21	0.19	0.14	0.21
S	0.029	0.119	0.098	0.109	0.167	0.156	0.172	0.115	0.162	0.133	0.122	0.158	0.113	0.177	0.172	0.086
Cl	0.084	0.061	0.072	0.076	0.054	0.058	0.056	0.070	0.054	0.067	0.060	0.067	0.066	0.062	0.057	0.067
H_2O[g]																
Total	100.84	98.99	98.81	99.02	99.92	99.15	98.26	98.97	98.16	99.36	98.18	99.53	98.47	98.75	97.79	97.68
S6+/Stotal	0.40	0.40	0.56	0.17	0.34	0.46	0.35	0.31	0.43	0.33	0.28	0.43	0.19	0.42	0.42	0.33
log fO_2 (ΔFMQ)[b]	1.0	1.0	1.3	0.5	0.9	1.1	0.9	0.8	1.0	0.9	0.8	1.0	0.6	1.0	1.0	0.9
Host Fo #		81.5	81.3	81.7	82.2	82.7	82.7	82.8	84.0	80.5	83.8	82.3	80.8	83.9	83.4	82.0
$Kd^{c}_{ol\text{-}melt}$		0.3	0.287	0.239	0.312	0.284	0.347	0.298	0.36	0.35	0.334	0.357	0.285	0.345	0.367	0.355
Adjusted melt inclusion compositions[d]																
SiO_2		49.40	49.68	49.96	49.15	49.23	48.67	49.48	48.90	49.81	48.26	49.43	47.98	48.75	48.33	49.44
TiO_2		1.27	1.39	1.44	1.20	1.22	1.16	1.29	1.16	1.36	1.16	1.48	1.26	1.07	1.15	1.28
Al_2O_3		16.93	17.06	15.57	18.62	18.05	17.26	16.16	18.09	17.25	18.34	18.15	15.50	18.22	18.10	16.70
Fe_2O_3		2.14	2.36	1.79	1.84	1.98	1.80	1.88	1.68	2.19	1.73	2.16	1.92	1.72	1.74	1.77
FeO		8.31	8.00	9.18	7.68	7.51	7.81	9.01	6.85	8.15	6.84	7.51	10.34	7.29	7.10	7.93
MnO		0.18	0.17	0.17	0.16	0.14	0.17	0.17	0.19	0.17	0.18	0.18	0.23	0.16	0.16	0.17
MgO		6.18	5.88	6.90	5.98	6.03	6.28	7.26	6.04	5.65	5.96	5.86	7.30	6.40	5.98	6.10
CaO		11.53	11.19	11.20	12.20	12.13	12.01	10.49	12.10	11.45	12.09	11.41	10.94	12.03	12.17	11.11
Na_2O		2.56	2.63	2.33	2.57	2.39	2.51	2.65	2.52	2.73	3.01	2.72	2.50	2.49	2.51	2.59
K_2O		0.31	0.33	0.32	0.29	0.27	0.29	0.34	0.28	0.34	0.30	0.31	0.31	0.30	0.28	0.32
P_2O_5		0.23	0.21	0.22	0.18	0.20	0.22	0.19	0.17	0.20	0.19	0.25	0.21	0.19	0.13	0.21
S		0.12	0.10	0.10	0.17	0.15	0.18	0.12	0.17	0.14	0.12	0.16	0.11	0.18	0.18	0.09
Cl		0.06	0.07	0.07	0.05	0.06	0.06	0.07	0.06	0.07	0.06	0.07	0.07	0.06	0.06	0.07
$X^{f}_{olivine}$		0.00	0.01	0.04	−0.01	0.01	−0.03	0.00	−0.04	−0.03	−0.02	−0.04	0.01	−0.03	−0.05	−0.04

Notes:[a] FeO as total Fe. [b]log $fO2$ (ΔFMQ) determined from Wallace and Carmichael (1994). [c]Kdol-melt determined from Sack et al. (1981). [d]See text for detailed explanation of adjustment of melt inclusion compositions. [e]Experiments performed at the IW oxygen buffer (all other experiments performed at the FMQ oxygen buffer). [f]Fraction of olivine (by wt) added or subtracted from the melt composition. [g]H_2O determined by SIMS (A. Kent, upd; Kent et al. (2002)). [h]CC02-1 adjusted melt compositions are not "real" compositions since the sulfur speciation used to determine oxygen fugacity has been altered by post entrapment modification. [i]Whole rock major element analysis conducted at Washington State University.

(continued on next page)

Table 2 (*continued*)

Locality	Izu backarc									Loihi Seamount						
Sample	31-7B									LO-02-04	LO-02-02					
ID	30-6-1	30-1-1	1.1	1.2	2.1	1.2	2.1	3.1	3.1	LO-02-04ii	1	2	3	15xglass-A-1	15xcrystal-A-3	15xcrystal-B-2
Temperature (°C)	1143	1143	1177	1177	1177	1206	1206	1206	1231	Matrix	Unheated	Unheated	Unheated	1200	1200	1200
Time (min)	30	30	10	10	10	10	10	10	10					15	15	15
Measured melt inclusion compositions																
SiO_2	49.46	48.61	48.09	47.89	48.47	48.39	48.07	47.09	47.82	49.30	47.55	47.92	48.41	48.47	47.49	47.56
TiO_2	1.20	1.27	1.07	1.09	1.13	1.16	1.02	1.01	1.02	2.24	3.16	3.14	2.87	2.13	2.79	2.20
Al_2O_3	18.22	15.01	15.45	16.20	16.07	14.90	15.03	14.35	14.60	12.17	12.44	12.42	12.38	11.49	11.66	10.48
FeO[a]	8.86	10.94	12.31	10.68	11.30	13.36	13.84	13.21	12.10	10.84	10.76	10.79	10.61	9.69	11.37	9.71
MnO	0.13	0.23	0.18	0.22	0.20	0.22	0.19	0.18	0.21	0.16	0.21	0.18	0.14	0.14	0.17	0.14
MgO	7.27	7.20	8.70	8.92	8.81	9.46	9.35	9.99	10.93	9.03	6.45	8.56	9.41	12.34	9.76	11.91
CaO	11.17	10.42	10.25	10.82	10.87	9.91	9.95	9.62	9.40	10.53	12.89	12.54	11.25	9.70	11.79	9.98
Na_2O	2.72	2.67	2.40	2.34	2.35	2.50	2.32	2.12	2.25	2.48	1.99	1.87	1.88	1.86	1.96	2.16
K_2O	0.30	0.35	0.28	0.27	0.24	0.29	0.26	0.26	0.27	0.59	0.58	0.37	0.60	0.55	0.37	0.43
P_2O_5	0.24	0.19	0.18	0.19	0.18	0.22	0.18	0.17	0.14	0.30	0.26	0.23	0.26	0.29	0.26	0.27
S	0.122	0.056	0.137	0.130	0.141	0.062	0.112	0.142	0.074	0.140	0.100	0.149	0.136	0.139	0.290	0.123
Cl	0.062	0.070	0.054	0.055	0.055	0.061	0.049	0.047	0.054	0.140	0.035	0.042	0.039	0.046	0.096	0.023
H_2O[g]										1.60				0.98	1.08	1.41
Total	99.88	97.03	99.10	98.84	99.82	100.51	100.36	98.19	98.87	99.52	96.43	98.21	97.99	97.84	99.09	96.40
S6+/Stotal	0.28	0.30	0.41	0.28	0.23	0.35	0.16	0.28	0.13	0.38, 0.45	0.24	0.23	0.17	0.36	0.28	0.31
log fO_2 (ΔFMQ)[b]	0.8	0.8	1.0	0.8	0.7	0.9	0.5	0.8	0.4	1.0, 1.1	0.7	0.6	0.5	0.9	0.8	0.8
Host Fo #	85.1	80.8	80.8	82.5	81.6	82.0	82.2	82.5	82.3		87.1	87.3	87.4	87.1	87.3	87.3
$Kd^c_{ol\text{-}melt}$	0.301	0.333	0.36	0.37	0.365	0.328	0.299	0.332	0.391		0.195	0.249	0.268	0.401	0.269	0.38
Adjusted melt inclusion compositions[d]																
SiO_2	49.47	48.87	48.60	48.42	49.00	48.65	48.07	47.37	48.60		46.76	47.49	48.13	50.55	47.65	50.28
TiO_2	1.20	1.30	1.12	1.16	1.20	1.19	1.02	1.04	1.12		2.86	2.98	2.78	2.41	2.72	2.50
Al_2O_3	18.24	15.40	16.25	17.16	16.95	15.31	15.03	14.82	15.93		11.24	11.79	11.98	13.00	11.37	11.94
Fe_2O_3	1.45	2.01	2.38	1.88	1.90	2.35	1.92	2.10	1.68		2.05	1.94	1.73	1.95	2.10	2.02
FeO	7.55	8.97	9.89	8.65	9.27	11.14	12.11	11.22	10.18		9.05	9.12	9.10	7.88	9.60	8.02
MnO	0.13	0.23	0.17	0.22	0.19	0.22	0.19	0.17	0.21		0.21	0.18	0.14	0.14	0.17	0.15
MgO	7.24	6.32	6.99	6.86	6.93	8.51	9.35	8.92	7.97		10.29	10.53	10.66	8.95	11.11	8.96
CaO	11.18	10.68	10.76	11.45	11.45	10.17	9.95	9.93	10.24		11.64	11.90	10.88	10.95	11.50	11.34
Na_2O	2.73	2.74	2.52	2.48	2.48	2.57	2.32	2.19	2.46		1.80	1.78	1.81	2.10	1.91	2.46
K_2O	0.30	0.36	0.30	0.29	0.25	0.30	0.26	0.27	0.29		0.53	0.35	0.58	0.62	0.36	0.49
P_2O_5	0.24	0.18	0.17	0.19	0.18	0.21	0.18	0.17	0.13		0.23	0.22	0.26	0.29	0.26	0.28
S	0.12	0.06	0.14	0.14	0.15	0.06	0.11	0.15	0.08		0.09	0.14	0.13	0.16	0.28	0.14
Cl	0.06	0.07	0.06	0.06	0.06	0.06	0.05	0.05	0.06		0.03	0.04	0.04	0.05	0.09	0.03
$X^f_{olivine}$	0.00	−0.03	−0.05	−0.06	−0.05	−0.03	0.00	−0.03	−0.08		0.10	0.05	0.03	−0.10	0.03	−0.09

Loihi Seamount			Quartzville (Oregon Cascades)							Cayuse crater (Oregon Cascades)						
LO-02-02			QV04-3B							CC02-1[h]						
30x-A-1	30x-B-1	30x-C-2	qvscoria	04-036-1	04-036-9	04-050-17.1	04-050-20.1	05-014-1	05-014-7	bulk rock[i]	03-015-26.1	03-015-47.1	03-015-77.1	03-041-8.1	03-041-9.1	03-041-13.1
1200	1200	1200	matrix	unheated	unheated	unheated	unheated	1112–1119	1112–1119		1218–1224	1218–1224	1218–1224	1218–1224	1218–1224	1218–1224
30	30	30						10	10		15	15	15	15	15	15
48.58	47.73	46.32	50.61	50.33	50.05	50.18	50.34	49.39	49.05	51.94	50.87	51.14	51.06	49.66	50.13	50.41
2.59	2.71	2.61	1.74	1.65	1.79	1.89	1.87	1.81	1.82	1.05	1.04	1.06	1.03	0.98	1.04	1.01
11.65	11.24	11.39	16.74	14.80	15.55	15.67	15.35	17.10	17.00	16.53	17.43	17.76	17.34	17.70	18.25	17.63
10.64	12.02	11.28	6.21	6.30	6.84	6.93	7.44	6.70	7.28	7.85	7.94	8.04	7.29	8.51	7.71	7.70
0.15	0.17	0.15	0.11	0.13	0.15	0.12	0.13	0.10	0.13	0.15	0.11	0.13	0.13	0.15	0.10	0.13
10.05	11.65	11.08	4.59	4.59	5.23	5.30	5.20	4.70	4.59	8.62	8.74	8.90	9.41	8.03	8.24	8.66
10.75	10.19	11.70	8.72	11.67	10.72	10.09	10.15	8.60	8.93	9.15	9.38	10.06	10.10	9.65	9.92	9.80
1.85	1.70	1.84	3.91	2.77	3.05	2.58	1.63	3.54	3.50	3.13	3.21	3.27	3.16	3.20	3.14	3.14
0.46	0.38	0.33	3.40	2.38	1.34	1.55	1.85	4.23	4.00	0.65	0.66	0.60	0.59	0.65	0.59	0.59
0.24	0.28	0.32	1.31	1.59	1.52	1.37	1.31	1.42	1.39	0.22	0.21	0.19	0.17	0.22	0.23	0.25
0.147	0.173	0.179	0.270	0.272	0.503	0.442	0.465	0.298	0.340	na	0.095	0.110	0.104	0.112	0.089	0.111
0.046	0.040	0.077	0.160	0.175	0.180	0.151	0.156	0.116	0.126	na	0.073	0.053	0.049	0.056	0.056	0.055
0.67	0.62	0.66														
97.80	98.91	97.92	97.77	96.66	96.93	96.28	95.89	97.99	98.15	99.29	99.75	101.31	100.44	98.91	99.49	99.48
0.31	0.18	0.18	0.68, 0.80	0.65	0.84	0.76	0.87	0.58	0.73		0.31	0.31	0.48	0.04	0.08	0.24
0.8	0.5	0.5	1.5, 1.8	1.4	1.9	1.7	2.0	1.3	1.6		0.8	0.8	1.1	−0.2	0.1	0.7
87.6	86.4	86.9		88.8	89.0	86.1	89.6	87.6	89.0		86.7	87.1	88.1	86.1	87.4	87.4
0.288	0.315	0.307		0.276	0.244	0.305	0.208	0.241	0.195		0.365	0.355	0.382	0.294	0.310	0.350
49.53	48.42	47.34		50.19	49.73	50.20	49.71	49.06	48.45		51.43	51.63	51.76	49.61	50.21	50.82
2.61	2.80	2.69		1.63	1.73	1.89	1.75	1.76	1.70		1.10	1.11	1.09	0.98	1.05	1.05
11.75	11.57	11.72		14.61	15.02	15.70	14.38	16.56	15.83		18.30	18.54	18.45	17.61	18.39	18.33
2.01	1.87	1.86		2.01	2.28	2.14	2.34	1.90	2.20		1.66	1.69	1.62	0.74	1.01	1.54
9.08	10.46	9.84		4.57	4.92	4.98	5.50	5.10	5.51		6.20	6.33	5.57	7.87	6.77	6.15
0.15	0.17	0.15		0.13	0.15	0.12	0.13	0.10	0.13		0.11	0.13	0.13	0.15	0.10	0.13
10.75	11.15	11.02		5.13	6.71	5.21	7.94	6.07	7.54		6.84	7.22	6.95	8.22	7.93	7.16
10.85	10.49	12.03		11.53	10.36	10.11	9.52	8.37	8.33		9.85	10.49	10.73	9.60	10.00	10.18
1.87	1.75	1.89		2.74	2.95	2.59	1.53	3.41	3.25		3.37	3.41	3.36	3.18	3.16	3.26
0.46	0.39	0.34		2.35	1.30	1.56	1.74	4.05	3.72		0.70	0.62	0.63	0.65	0.60	0.62
0.24	0.28	0.32		1.58	1.48	1.37	1.24	1.50	1.31		0.21	0.19	0.17	0.22	0.23	0.26
0.15	0.18	0.18		0.27	0.49	0.44	0.44	0.28	0.32		0.10	0.11	0.11	0.11	0.09	0.12
0.05	0.04	0.08		0.17	0.17	0.15	0.15	0.11	0.12		0.08	0.05	0.05	0.06	0.06	0.06
0.01	−0.02	−0.01		0.013	0.034	−0.002	0.063	0.043	0.069		−0.048	−0.043	−0.060	−0.005	−0.001	−0.038

curve defined by Wallace and Carmichael (1992) are assumed to be breached and therefore no longer reflect the initial trapped melt composition. For heated melt inclusions in this study, only inclusions which retain sulfur concentrations at or above the sulfide saturation curve are considered further. In addition, olivine hosted melt inclusions included in this study generally have round to ovoid shapes, characteristic of primary inclusions. Groundmass compositions and sulfur speciation results are reported for 31-7B, LO-02-04 (equivalent to LO-02-02), and QV04-3B. No glassy groundmass was available from CC02-1, however the bulk rock composition is provided in Table 2 for comparison.

Melt inclusion compositions have been re-calculated to be in equilibrium with their host olivine using the measured sulfur speciation and empirical curve defined by Wallace and Carmichael (1994) to determine the oxidation state and following procedures in Sobolev and Chaussidon (1996) and Rowe et al. (2006). The empirical curve defined by Jugo et al. (2005a) is not utilized in this study to determine oxidation state. Although the Jugo et al. (2005a) curve may prove to be more robust, taking into account the presence of sulfite, too few studies on the proportion of sulfite in oxidized magmas exist to for this to be well constrained at this time. Applying the oxygen fugacity and experimental temperatures to the Sack et al. (1980) formulation, the Fe^{2+}/Fe^{3+} is calculated for the melt inclusions. Assuming a constant olivine-melt Fe/Mg equilibrium of 0.3 the melt inclusion compositions are numerically adjusted by incrementally adding or subtracting olivine from the melt composition (Table 2; Roedder and Emslie, 1970). Since the assumption is made that the analyzed melt inclusions are water-bearing, analyzed compositions are not normalized to 100% (anhydrous) prior to adjustment of compositions. However, water (estimated as the difference between analytical totals and 100%) has been added prior to recalculation to maintain mass balances while accurately reflecting compositional variability. In the case of heated Loihi inclusions where water contents are known, melt inclusion compositions are normalized to 100% prior to adjustment.

Re-equilibration between the host olivine and the melt inclusion is a significant concern when heating melt inclusions (Danyushevsky et al., 2000). A high K_D (>0.3) may indicate re-equilibration, or iron loss, has occurred, however the olivine-melt Fe/Mg equilibrium is also used in heating experiments as a monitor of over/under-heating. Iron concentrations of heated melt inclusions compared to that of matrix glass or whole rock FeO* concentrations (overheating normally results in anomalously high FeO∗ while re-equilibration results in anomalously low FeO∗) are therefore utilized in conjunction with the calculated K_D values to monitor for olivine-melt re-equilibration. Based on these comparisons, re-equilibration does not appear to have significantly affected the melt compositions from samples 31-7B, LO-02-02, and QV04-3B. Analytical results are summarized below for each of the four samples.

4.1. 31-7B

Sulfur concentrations (980–1670 ppm) and speciation (17–56% relative proportion sulfate) vary significantly in unheated melt inclusions. Only one unheated melt inclusion recorded a sulfur speciation (17% relative proportion sulfate) significantly different from other unheated inclusions and matrix glass. With decreasing sulfur concentrations, MgO, CaO, and Al_2O_3 also decrease while SiO_2, Cl, K_2O, TiO_2 and P_2O_5 concentrations increase (Table 2). These variations in major element composition in the naturally quenched melt inclusions, coinciding with decreasing sulfur concentration, suggest crystallization of the melt is occurring during degassing.

Olivine crystallization temperature for Fo_{82} olivine in Izu basalt 31-7B is estimated from MELTS at ~1147 °C (2 wt.% H_2O, 0.1 GPa; Ghiorso and Sack, 1995; Asimow and Ghiorso, 1998). Heating experiments conducted near the estimated olivine crystallization temperature for 10 min at the IW oxygen buffer (1133 °C) and 10–30 min at FMQ (1143 °C) have measured S^{6+}/S_{total} in undegassed melt inclusions, indistinguishable from unheated inclusions (Fig. 5B). This suggests that heating of inclusions near the olivine crystallization temperature does not change the redox state of the melt inclusion for short duration experiments (<30 min).

Melt inclusions heated to temperatures above the olivine crystallization temperature (1177 °C, 1206 °C, and 1231 °C) record a lower proportion of sulfate with increasing degree of overheating (Fig. 5A). Only one melt inclusion heated at 1231 °C retained measurable sulfur (740 ppm) and chlorine (540 ppm), however despite a major element composition similar to other melt inclusions, sulfur concentrations are significantly lower than measured in other heated and unheated melt inclusions suggesting that some sulfur loss may have occurred. Since no visible fractures are evident, sulfur loss is believed to have occurred prior to entrapment within the olivine host. The absence of preserved, undegassed melt inclusions in olivine grains heated to ~90° above the olivine crystallization temperature may

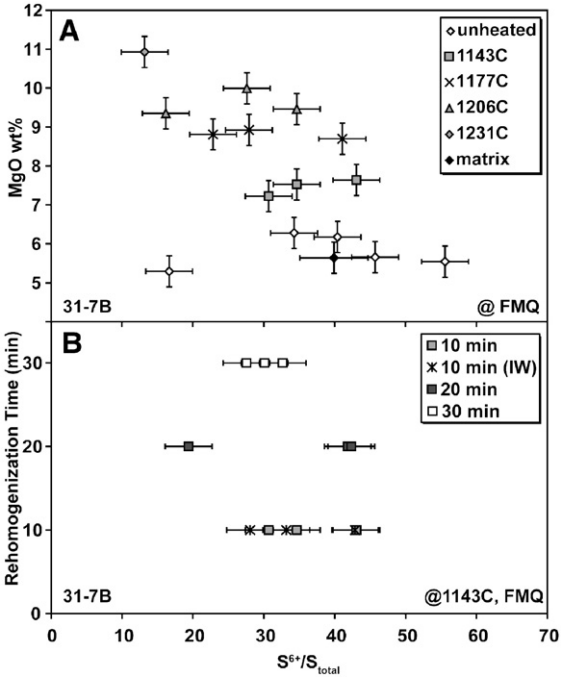

Fig. 5. Reheating experiments for sample 31-7B. (A) Measured MgO wt.% of inclusions reheated at constant time and oxygen fugacity (~FMQ) with variable temperature versus sulfur speciation. (B) Sulfur speciation of inclusions reheated at constant temperature with variable time. All heating experiments were conducted at the FMQ oxygen buffer except where specifically stated (i.e. IW). Error bars are 2 σ for sulfur concentrations, based on repeat analysis of LO-02-04, and 1 σ for sulfur speciation, determined by repeat analysis of glass K 14-3.

be a function of the increased pressure within inclusions at higher temperatures resulting in a greater likelihood of inclusions breaching and degassing during heating.

Measured MgO wt.% in melt inclusions increases with degree of overheating, from 5.29–6.28 wt.% in naturally quenched inclusions to 10.93 wt.% at 1231 °C (~90 °C above the olivine crystallization temperature; Table 2; Fig. 5A). The increase in MgO content of the inclusions coincides with an increase in calculated olivine-melt K_D (see methods for discussion of this calculation), indicating excess dissolution of olivine (~8 wt.%) into the melt during overheating.

4.2. LO-02-02

In naturally quenched LO-02-02 melt inclusions, sulfur speciation varies from 17–23% relative proportion sulfate, compared to 37–44% in LO-02-04 groundmass glass (Fig. 6). The range in sulfur speciation, while distinctly lower than that of the groundmass glass is comparable to the range observed in melt inclusions heated for 30 min (17–30% relative proportion sulfate) and only somewhat lower than that measured in inclusions heated for 15 min (28–35% relative proportion sulfate; Fig. 6). In addition, there is an overall increase in the proportion of sulfate with increasing water content in heated inclusions and groundmass glass (water contents are not available for unheated inclusions in this study). Calculation of an average olivine crystallization temperature using the MELTS algorithm indicates a crystallization temperature of ~1208 °C (1.6 wt.% H_2O, 0.1 GPa; Ghiorso and Sack, 1995; Asimow and Ghiorso, 1998), similar to the heating temperature of 1200 °C, indicating these inclusions were not overheated. The correlation of sulfur speciation between inclusions heated for 30 min with unheated inclusions may indicate, as with Izu basalt 31-7B, that sulfur speciation is not changing appreciably during heating. Despite the decrease in water concentration with increase time of heating, characteristic of H diffusion and water loss, all of the heated inclusions fall within the range of sulfur speciation defined by the groundmass and unheated inclusions (Fig. 6).

Sulfur (0.1–0.29 wt.%) and chlorine (0.023–0.096 wt.%) concentrations in heated and unheated melt inclusions both increase with increasing Cl/K_2O (0.06–0.23; Fig. 7). Cl/K_2O has previously been identified in Loihi glasses as an indicator of assimilation of a seawater derived component (Kent et al., 1999a,b). This correlation may then indicate that changes in the sulfur concentration, and therefore the sulfur speciation, may also be attributed to assimilation. However, unheated inclusions which have relatively low Cl/K_2O ratios, and therefore are interpreted to not be significantly influenced by assimilation, have relative sulfate proportions (17–23%) that are significantly lower than from

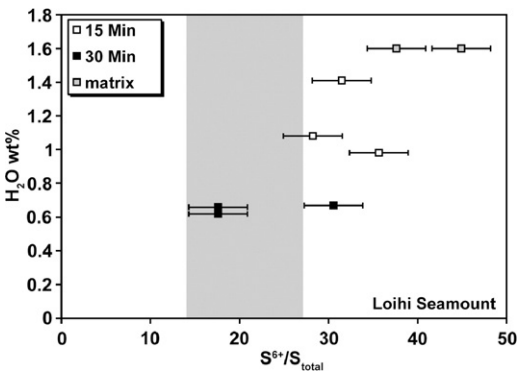

Fig. 6. Sulfur speciation versus melt inclusion water content for LO-02-02. Also included are water contents and sulfur speciation measurements of LO-02-04 groundmass (see text). Grey field is the range of sulfur speciation observed in naturally quenched melt inclusions.

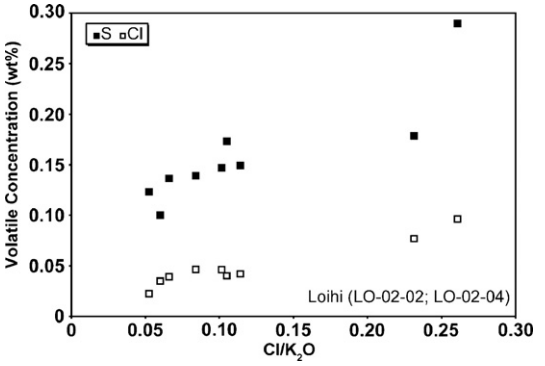

Fig. 7. Sulfur and chlorine versus Cl/K_2O in matrix glass and heated and naturally quenched inclusions from LO-02-02 and LO-02-04.

inclusions heated for 15 min (32–36%) with similar Cl/K_2O ratios. Therefore the variability in sulfur speciation in the heated melt inclusions may be a function of multiple processes resulting as a combination of assimilation of seawater or a Cl-rich brine as indicated by the Cl/K_2O ratio and H diffusion (water loss) generating more oxidized conditions (see discussion below; Figs. 6 and 7).

4.3. QV04-3B

Sulfur speciation (S^{6+}/S_{total}) in groundmass glass, and heated and naturally quenched melt inclusions ranges from 58 to 86% relative proportion sulfate. In addition, sulfur (0.50–0.27 wt.% S) and chlorine (0.18–0.12 wt.% Cl) concentrations both decrease as a function of decreasing S^{6+}/S_{total} (Fig. 8; Table 2). Total sulfur concentrations, in conjunction with measured S^{6+}/S_{total} ratios indicate that as total sulfur concentrations decrease, sulfide concentrations stay relatively constant (0.06 to 0.1 wt.% sulfide) while sulfate concentrations drop significantly from 0.4 wt.% sulfate to 0.17 wt.% sulfate.

Naturally glassy melt inclusions were heated at temperatures (1112–1119 °C) near crystallization temperatures of 1100–1115 °C estimated through heating experiments and numerically with the COMAGMAT application (Rowe et al., 2006; Ariskin et al., 1993). Major element compositions differ between naturally quenched and heated melt inclusions, especially evident in K_2O and CaO (Table 2). Two of the naturally quenched melt inclusions are out of equilibrium with their host olivine grains as indicated by low olivine-melt K_D values (Table 2). The low K_D values may be explained by crystallization of ~3 to 6 wt.% olivine on the walls of the inclusion, however correcting for this crystallization does not adequately explain the compositional differences between the heated and unheated inclusions (Table 2). A bulk FeO* concentration of 6.53 wt.%, similar to the total FeO measured in melt inclusions, coupled with the low olivine-melt K_D values (<0.30) suggests Fe-loss has not affected these naturally quenched or heated inclusions (Table 2; Rowe et al., 2006).

While limited sampling of QV04-3B presented here may suggest two populations of inclusions, a more thorough set of analyses illustrates a complete spectrum between the high K_2O and low K_2O melt inclusions (Fig. 9; Rowe, 2006). SiO_2, and to a lesser extent K_2O, in naturally quenched melt inclusions generally increases with decreasing sulfur content (Fig. 9), however Na_2O and K_2O concentrations are relatively variable. The lack of a significant correlation though between total alkali content and sulfur concentration suggests alkali metals are not strongly influencing sulfur solubility. Major element concentrations of scoria glass overlap with more evolved melt inclusions and are consistent with fractional crystallization of dominantly olivine from more primitive melt inclusion compositions (Rowe, 2006). These correlations, coupled with similar trace element ratios and concentrations suggests that these inclusions are derived from the same magma

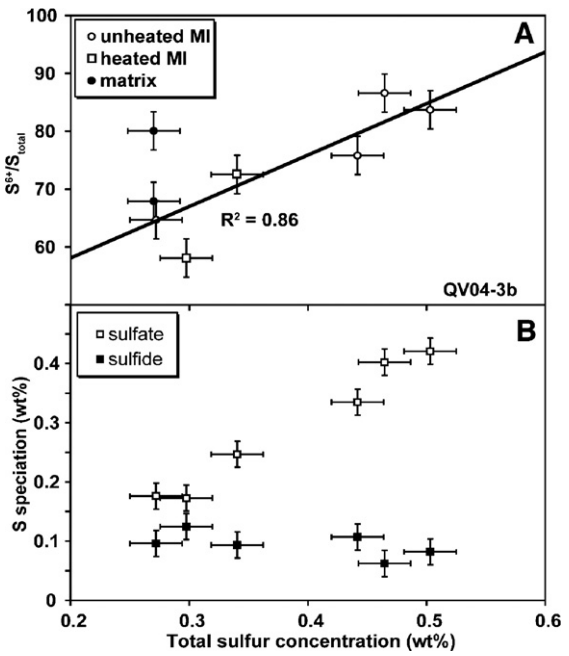

Fig. 8. (A) Sulfur speciation versus total sulfur content for naturally quenched (open circles) and heated (open squares) melt inclusions and matrix glass (solid symbols) from sample QV04-3B. Error bars same as Fig. 5. (B) Weight percent sulfide (solid symbols) and sulfate (open symbols) versus total sulfur concentration for QV04-3B reheated and naturally quenched melt inclusions. Error bars are 2σ.

source (Rowe et al., 2006; Rowe, 2006). High K_2O melt inclusions and scoria glass coincide with lower S and Cl concentrations and may therefore record late crystallization concurrent with degassing. Despite the apparent differences in major element composition, heated QV04-3B melt inclusions presented here illustrate the important point that the measured sulfur speciation does not vary significantly between heated and unheated melt inclusions at similar sulfur concentrations.

4.4. CC02-1

Crystalline melt inclusions from Cayuse crater basalt were rehomogenized at temperatures between 1218–1224 °C near the olivine crystallization temperature of ~1227 °C estimated from MELTS modeling (0.1 GPa, 1 wt.% H_2O; Ghiorso and Sack, 1995; Asimow and Ghiorso, 1998). Measured S^{6+}/S_{total} ranged from 3% to 48% relative proportion sulfate in the rehomogenized melt inclusions. Major element compositions of rehomogenized melt inclusions correlate well with measured sulfur speciation (Fig. 10A–C). In contrast to inclusions from samples 31-7B and QV04-3B, sulfur (0.09–0.1 wt.% S) and chlorine (0.05–0.07 wt.% Cl) however vary little between inclusions and show no correlation to the measured S^{6+}/S_{total} (Fig. 10D).

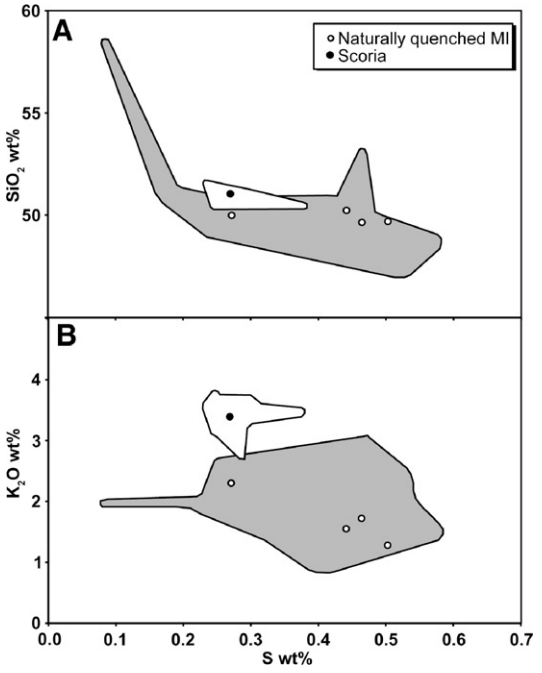

Fig. 9. Sulfur concentration versus (A) SiO_2 and (B) K_2O in naturally glassy melt inclusions and scoria. Fields define the complete range of compositions observed in scoria (white) and naturally glassy melt inclusions (grey) defined by Rowe (2006).

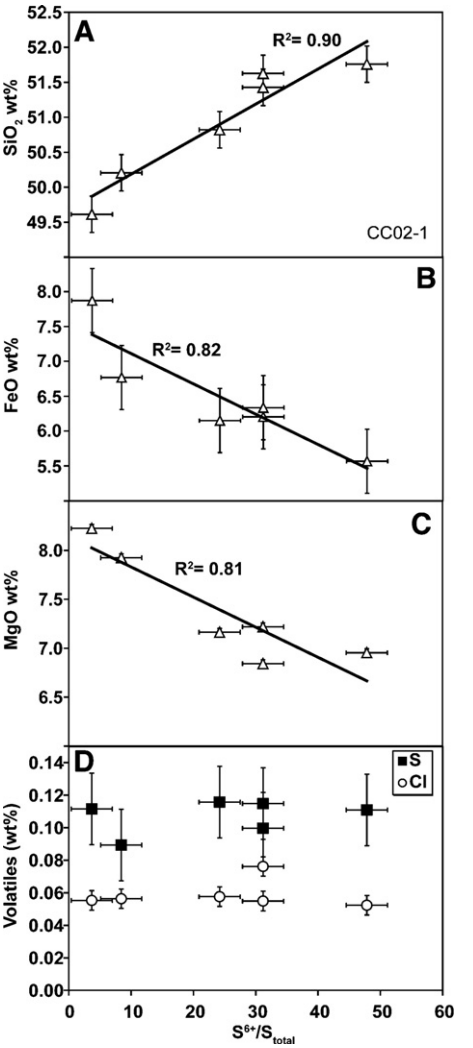

Fig. 10. Major element variation (and Cl and S) as a function of sulfur speciation for sample CC02-1. Major elements have been numerically adjusted using the measured melt sulfur speciation to determine oxidation state and Fe^{2+}/Fe^{3+} after Sack et al. (1980). Error bars are same as Fig. 5 (2σ for major elements).

Measured FeO* concentrations in melt inclusions vary from 7.29 to 8.51 wt.% FeO*, similar to iron concentrations from whole rock analysis (7.85 wt.%; Table 2). In addition, MgO concentrations increase significantly from 8.03 to 9.41 wt.% MgO, with high MgO concentrations correlating to low FeO concentrations (Fig. 11). The variations in MgO cannot be attributed to overheating of the melt inclusions as FeO* would also be expected to increase (based on ~12 wt.% FeO in Fo_{87} olivine). The covariation of FeO* and MgO therefore may be the result of re-equilibration of the host olivine with the melt inclusion (Danyushevsky et al., 2000).

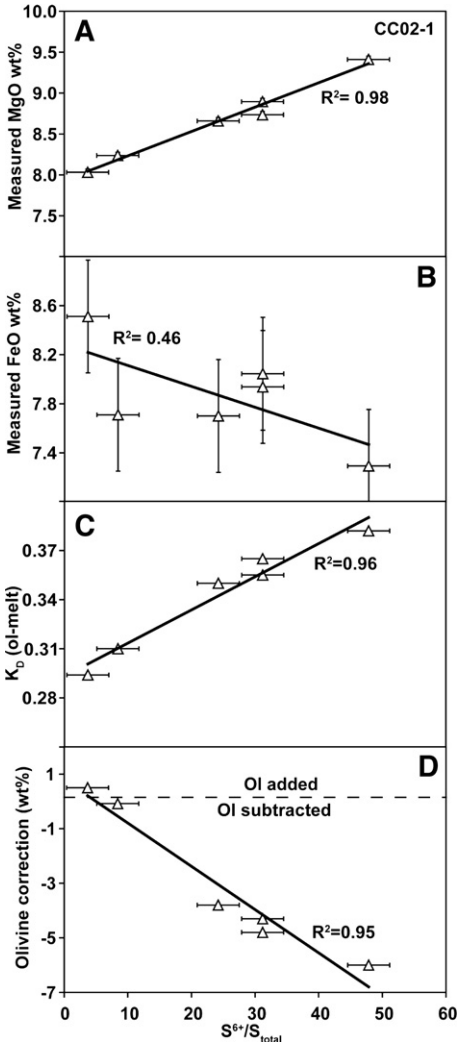

Fig. 11. Measured (A) MgO wt.% and (B) FeO wt.%, and (C) olivine-melt K_D versus sulfur speciation for sample CC02-1. Olivine-melt K_D calculated based on Fe^{2+}/Fe^{3+} determination after Sack et al. (1980) with log fO_2 from sulfur speciation measurements. (D) Olivine correction (in wt.%) required to adjust the melt composition to be in equilibrium with the host olivine assuming a K_D of 0.30 (Roedder and Emslie, 1970). Error bars for MgO and FeO wt% are 2 σ; sulfur speciation error same as previous figures.

Both measured and adjusted melt inclusion major element compositions define correlations with the relative proportion sulfate (Figs. 10 and 11). Melt inclusion compositions have been adjusted to be in equilibrium with their host olivine as previously described. Re-equilibration between the host olivines and the inclusions has not been corrected for in Table 2; while this does impact the adjusted compositions the resulting trends are not significantly altered. Adjusted melt inclusion concentrations of SiO_2 (51.76–49.61 wt.%), CaO (10.73–9.6 wt.%), and Fe_2O_3 (1.62–0.74 wt.%) have well defined positive correlations with sulfur speciation while Na_2O (3.41–3.16 wt.%) and TiO_2 (1.11–0.98 wt.%) have weak positive correlations. Adjusted MgO (8.22–6.95 wt.%) and FeO (7.87–5.57 wt.%) concentrations define negative correlations with increasing proportion of sulfate (Fig. 10). Importantly, the adjusted MgO trend with proportion of sulfate is opposite that of the measured MgO compositional trend (Figs. 10C and 11A).

Compositional trends evolving from adjustment of melt inclusion compositions to be in equilibrium with their host olivine grains appear to be a result of the oxygen fugacity used to determine the Fe^{3+}/Fe_{total} in the melt. Oxygen fugacity, as previously described is calculated from measured sulfur speciation that in CC02-1 melt inclusions varies from 4% to 48% relative proportion sulfate, resulting in a range of fO_2 from −0.2 to 1.1 log units (ΔFMQ). The large variation in oxygen fugacity is reflected in the calculated olivine-melt K_D which in turn results in the variation of olivine added to the melt (up to 6 wt.% removed; Table 2; Fig. 11C). Instead of adjusting melt compositions with the measured sulfur speciation, if the lowest fO_2 (coinciding with the olivine-inclusion pairs which are in equilibrium) is used to recalculate the melt compositions, the compositional trends with proportion of sulfate disappear. This suggests that the compositional variation is an artifact of a measured sulfur speciation that has been altered by post-entrapment processes and therefore does not reflect the oxidation state at the time of inclusion entrapment.

5. Discussion

5.1. Inclusion v. matrix

It has been suggested that high sulfate proportions in primitive melt inclusions are largely the result of post-entrapment modification of melt inclusions (Metrich et al., 2005). To test this claim, the S^{6+}/S_{total} of olivine-hosted naturally glassy melt inclusions and coexisting glassy matrix material is compared for samples 31-7B and QV04-3B. Naturally glassy melt inclusions are found to correlate well with matrix glass measurements, however in general have a wide range in S^{6+}/S_{total} compared to the variation in sulfur speciation in the matrix glass (Fig. 12).

There is a large discrepancy between S^{6+}/S_{total} from Loihi melt inclusions and matrix glass from sample LO-02-04. As was previously discussed, the high Cl/K_2O and H_2O of the matrix glass has been interpreted as indicative

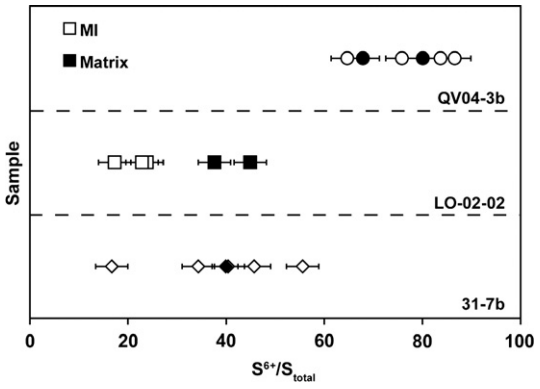

Fig. 12. Sulfur speciation measured from both matrix glass and melt inclusions for samples L0-02-02 (Loihi), QV04-3B (Quartzville basalt) and 31-7B (Izu backarc basalt). Solid symbols are matrix glass and open symbols are melt inclusions. Note that in general melt inclusions depict a wider range in sulfur speciation than observed in the matrix glass. Error bars same as Fig. 5.

of assimilation of a seawater derived brine in this lava (Kent et al., 1999a,b). A consequence of assimilation in this case appears to be an increase in the oxidation state of the matrix glass. The lower oxidation state and proportion sulfate, recorded by the naturally glassy inclusions suggests that they retain a S^{6+}/S_{total} of the melt prior to significant oxidation resulting from assimilation.

5.2. Post entrapment modification and rehomgenization

Several mechanisms are possible for altering the oxidation state and sulfur speciation of melt inclusions following entrapment in olivine phenocrysts and during rehomogenization. Since crystallization, olivine-melt re-equilibration, and H diffusion are commonly observed mechanisms for altering melt inclusion compositions, we will focus on the effects of these post-entrapment processes in modifying the sulfur speciation of the melt inclusions.

Rehomogenization of melt inclusions can be a useful technique for determining glass compositions prior to significant degassing, assimilation or crystallization when naturally glassy melt inclusions are not available. However, little is known about the effects of inclusion rehomogenization on the oxidation state of melt inclusions. Understanding the effects of experimental run time and temperature is essential for rehomogenization experiments as it has been suggested that, in addition to other post-entrapment mechanisms for modification, both variables may influence oxidation states of melt inclusions.

Whether melt inclusions behave as open or closed systems with regards to oxygen is also a significant factor with regard to post-entrapment processes and rehomogenization. Previous studies have suggested that inclusions behave as open systems with regard to oxidation state (for example: Danyushevsky et al., 2002) and we do not dispute the likelihood of open system exchange on some time scale. Perhaps a more significant factor then whether the system is open or closed to oxygen is the rate at which oxygen may exchange or diffuse through the olivine host. Previous studies of oxygen diffusion in forsteritic olivine have determined that oxygen diffusion coefficients at ~1200 °C are at least two log units lower than for Fe and Mg (Gerard and Jaoul, 1989; Ryerson et al., 1989). A low diffusion coefficient ($\sim 10^{-19}$ m^2/s), coupled with a relatively small compositional gradient (inclusion/olivine ratio of ~1.05 at.% O) suggests that while oxygen diffusion does occur the rates are significantly lower than that of Fe or Mg re-equilibration. It is unlikely then that for short duration (<15 min) heating experiments significant diffusion of oxygen occurs. Oxygen diffusion however may become a more significant concern for inclusions which have maintained high temperatures long enough to have re-equilibrated (Fe–Mg) with their host olivines.

Olivine oxidation, resulting in the formation of magnetite, is a function of multiple variables including, temperature, fO_2, Fe-content, and reaction rates, with transformation rates increasing at higher temperatures (Putnis, 1979; Gualtieri et al., 2003). Oxidation of olivine, while occurring rapidly on the outer surface of olivine grains during heating experiments at oxygen fugacities above FMQ, is only observed within breached inclusions, likely reflecting higher oxygen diffusion rates through melt or along fractures.

Fractional crystallization has the potential to modify magmatic oxidation states by removal of ferrous iron (Fe^{2+}) through crystallization of early silicate phases (olivine and clinopyroxene) resulting in an increase in the system's $Fe^{3+}/Fe^{2+}$and oxidation state (Carmichael and Ghiorso, 1986). A similar process is likely to occur in melt inclusions during cooling as the host mineral (in this case olivine) crystallizes on the mineral-inclusion boundary. For example, by adding 13 wt.% olivine to naturally quenched melt inclusion 31-7b (#15) a decrease in oxygen fugacity of 0.13 log units is produced. However, the degree to which the fO_2 of the inclusion will change during crystallization is a function of the initial Fe^{2+}/Fe^{3+} of the melt (see Fig. 2 in Mathez, 1984). This suggests that crystallization of olivine (increasing Fe^{3+}/Fe^{2+}), or melting (decreasing Fe^{3+}/Fe^{2+}) in the case of heating experiments, will not significantly impact the oxidation state of the melt inclusion.

Fe-loss, or olivine-melt re-equilibration, has perhaps a greater potential to alter the oxidation state of melt inclusions. Described in detail by Danyushevsky et al. (2000), olivine-melt re-equilibration results in an increase in the MgO content and a decrease in FeO in the melt. This process may have several consequences for the oxidation state of melt inclusions. As a result of Fe-loss, the Fe^{2+}/Fe^{3+} will decrease, thus changing the oxidation state. Additionally, since the ferrous iron content decreases, sulfides may crystallize from the melt as sulfide solubility is strongly dependant of ferrous iron concentration, thus increasing the S^{6+}/S_{total} (Danyushevsky et al., 2002; Wallace and Carmichael, 1992). The combined effect of these two processes would be an apparent increase in the oxidation state of the melt inclusion.

As with Fe-loss, diffusion of hydrogen also has the potential to result in oxidation of melt inclusions. Previous experimental studies have demonstrated that at temperatures greater than 1100 °C water may dissociate allowing hydrogen to rapidly diffuse out of the inclusion and host olivine (for example: Hauri, 2002; Danyushevsky et al., 2002). Diffusion of hydrogen following dissociation results in excess oxygen, allowing the melt to become progressively more oxidized and again may promote the formation of sulfide globules (Fig. 13; Sato and Wright, 1966; Mathez, 1984; Metrich et al., 1999). Because heating experiments presented in this study were conducted in a H_2-bearing furnace atmosphere diffusion rates for hydrogen may depend on the pressure of inclusion entrapment, water content, and oxygen fugacity of the furnace atmosphere (lower fO_2 equates to a higher proportion of H_2). As such, quantitative determination of the rates of oxidation to inclusions from H diffusion out of the melt may not be possible from these experiments. However for the example of sample 31-7B it should be reiterated that at temperatures appropriate for reheating of inclusions no significant difference between the naturally quenched inclusions and those reheated at the FMQ and IW buffers, despite a significantly greater volume of H_2 gas present in the furnace atmosphere at the IW oxygen buffer, is evident.

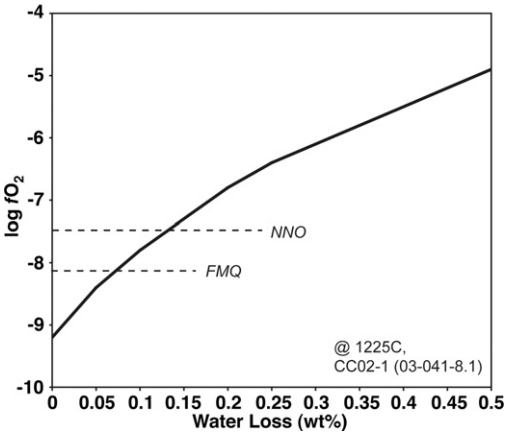

Fig. 13. Calculated curve for the oxidation of CC02-1 melt inclusion (03-041-8.1) based on water loss, assuming complete hydrogen diffusion upon dissociation of water. Oxygen fugacity was calculated at 1225 °C using the Sack et al. (1980) formulation. FMQ and NNO oxygen buffers shown for comparison.

An additional concern is that at higher temperatures (greater amount of overheating) rates of diffusion of both H and O will increase (Gerard and Jaoul, 1989; Ryerson et al., 1989). Reheating experiments on 31-7b (disregarding inclusions which may have experienced sulfur loss) suggest that there is significantly greater reduction of sulfur in the overheated melt inclusions than can be explained by fractional melting alone (Fig. 5A). Since H diffuses relatively rapidly through both the melt and olivine host, at sufficiently high temperatures in the presence of a H_2-bearing furnace atmosphere the melt inclusion may partially re-equilibrate with the furnace atmosphere (~FMQ) thus explaining the trend of melt oxidation state towards FMQ and the greater deviation from naturally quenched samples than could be explained by fractional melting (Fig. 5A). The higher pressure of the melt inclusion should promote H diffusion out of the inclusion for water bearing inclusions (Danyushevsky et al., 2002), never-the-less, a distinct trend towards the FMQ oxygen buffer (more reduced) is observed at higher temperatures.

Melt inclusions from sample CC02-1 provide a potential example to test both Fe-loss and H diffusion. As previously discussed, CC02-1 rehomogenized inclusions appear to have experienced minor Fe-loss (Fig. 11). Using a program created by L. Danyushevsky for reconstructing melt compositions that have experienced Fe-loss as a result of re-equilibration in conjunction with the Sack et al. (1980) formulation for calculating oxygen fugacity from melt compositions allows us to determine the effects on fO_2 from Fe-loss. Based on the recalculation of CC02-1 inclusion (03-015-77.1) correcting for 0.85 wt.% Fe-loss equates to an increase of fO_2 by 0.6 log units. While significant, this does not account for the total 1.3 log unit variation in oxidation state recorded by the sulfur speciation in these melt inclusions. In the absence of sulfide globules in the rehomogenized inclusions, this requires an additional means of increasing the oxidation state. If instead of Fe-loss, the assumption is made that the increase in oxidation state is the result of H diffusion, then dissociation

of only ~0.13 wt.% H_2O can cause the observed shift in oxidation state and the associated changes in sulfur speciation for this melt composition (Figs. 10 and 11). While this is not conclusive proof of oxidation by H diffusion, this example demonstrates that the dissociation of H_2O, as previously demonstrated by Mathez (1984), provides an excellent mechanism for the oxidation of melt inclusions. Additionally, the large potential change in sulfur speciation as a result of water dissociation and hydrogen diffusion (Fig. 13) makes determining sulfur speciation by microprobe an excellent technique for monitoring water-loss in melt inclusions without having to measure D/H ratios (i.e. Hauri, 2002).

5.3. Degassing

In most basaltic magmas, SO_2 (sulfur as sulfite) is the dominant sulfur-bearing gas phase, although higher fH_2O can result in generation of H_2S as a dominant gas phase (Carroll and Webster, 1994). However, we do not know how much of the S in SO_2 gas comes from oxidation of S^{2-} in the melt as opposed to the reduction of S^{6+} (P. Wallace, personal communication). Large ranges in measured sulfur speciation in naturally quenched, glassy melt inclusions may be related to degassing of the melt synchronous with entrapment in the olivine host crystals. If sulfide is preferentially lost through degassing, a possible mechanism proposed by Anderson and Wright (1972) and Wallace and Carmichael (1994) when $SO_2/H_2S \gg 1$ is the reduction of iron through the relationship:

$$S^{2-}_{(melt)} + 2Fe_2O_{3(melt)} = 4FeO_{(melt)} + SO_{2(gas)} \quad (5)$$

A similar mechanism may describe the reduction of sulfate to form SO_2 if again it is assumed that iron is the reducing agent for the sulfur in the melt:

$$SO^{2-}_{4(melt)} + 4FeO_{(melt)} = 2Fe_2O_{3(melt)} + SO_{2(gas)} \quad (6)$$

Sulfur concentrations from scoria and melt inclusions (naturally glassy and those heated near liquidus temperatures) in sample 31-7B range from 1767 ppm to 294 ppm (Fig. 14; Table 2). The similarity of slopes between linear trend lines suggests that sulfur speciation is not varying significantly during sulfur loss. Since both sulfide and sulfate are decreasing as total sulfur concentration decreases, the most probable explanation, in the absence of crystallized sulfur-bearing phases is that melt inclusions are recording shallow degassing, culminating with the low S groundmass. In the example of 31-7B however it is important to point out that these inclusions suggest sulfur speciation is not changing systematically as a result of degassing. It should be reiterated that major element concentrations record crystallization concurrent with degassing such that degassing alone may not be the only factor influencing the sulfur speciation.

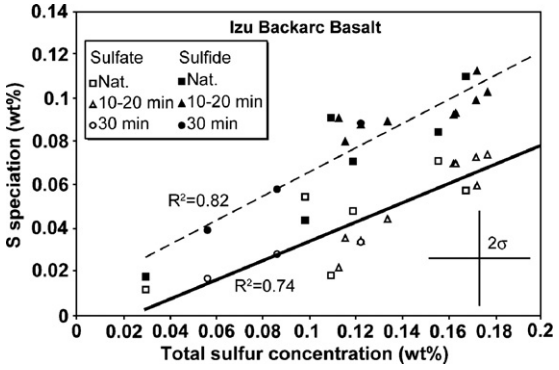

Fig. 14. Total sulfur concentration versus concentrations of sulfide and sulfate (determined from sulfur speciation) from sample 31-7B naturally glassy melt inclusions, inclusions heated at 1133 °C and 1143 °C, and scoria. The dashed line is a linear best fit through sulfide concentrations and the solid line is a best fit through sulfate concentrations. Error bars are 2σ.

Disregarding heated melt inclusions in sample QV04-3B which are compositionally different from the naturally quenched inclusions, there is a nearly 50% decrease in S concentration, from 5000 ppm to 2700 ppm S, recorded in naturally glassy melt inclusions and scoria glass. This decrease in sulfur concentration, in contrast to sample 31-7B, coincides with a decrease in S^{6+}/S_{total} (0.87 to 0.65) indicating sulfate is preferentially lost (Fig. 8B). In addition to degassing, several explanations for this behavior may be plausible. Micro-apatite grains with high sulfur cores (as indicated by electron microprobe X-ray mapping) observed in the groundmass of the lava may explain the decreasing sulfate concentrations, however no micro-apatite is observed in the scoria groundmass. As previously discussed, alkali metal content does not correlate with sulfur concentrations, despite prior observations that sulfur solubility and speciation may correlate with alkali and alkaline metals (Carroll and Webster, 1994). Another possible mechanism for decreasing the sulfur concentration is through varying the pressure of inclusion entrapment. Experiments using El Chichon trachyandesite material (summarized by Carroll and Webster, 1994), indicate that at comparable temperatures sulfur solubility decreases from ~5000 to ~3000 ppm in anhydrite-saturated experiments over a pressure range of 4 to 2 kbar. The absence of sulfate-bearing phases (i.e. anhydrite) in QV04-3B melt inclusions or in the scoria suggests that if sulfur solubility is decreasing as a function of pressure that

sulfate is likely forming a vapor phase. Shallow degassing therefore appears to be the most plausible explanation for decreasing sulfur concentrations in melt inclusions and scoria glass.

Gurenko and Schmincke (2000) reported that variations in sulfur speciation and sulfur concentration could not be attributed solely to degassing processes and that the variations likely were also the result of intrinsic variation in the Gran Canaria magmatic system. However, in the case of the Gran Canaria, a large variation in major element compositions also is present (i.e. 10.3 to ~3.75 wt.% MgO), supporting their results which indicate the likelihood that variations in sulfur speciation are a result of both degassing and mixing with other magmas to produce the observed variability. In contrast, inclusions from samples 31-7B and QV04-3B present a wide range in sulfur concentrations and speciation with comparatively little variation in major element composition. While other processes may be influencing the sulfur speciation in these naturally quenched inclusions, we feel that the most plausible cause for the variability in sulfur concentration and speciation is shallow degassing during entrapment of inclusions.

Naturally quenched melt inclusions from samples 31-7B and QV04-3B illustrate a key challenge for tracking changes in magmatic oxidation state during degassing, in that the oxidation state of the gas phase does not necessarily coincide with the oxidation state of the melt, resulting in changing sulfur speciation as degassing progresses. Regardless, because these inclusions are trapped at high pressures, high sulfur melt inclusions may provide the best estimate of magmatic oxidation states prior to significant degassing of sulfur and chlorine species.

6. Conclusion

Data presented here is the first attempt at characterizing the variations in sulfur speciation in melt inclusions as a result of natural magmatic processes, post entrapment modification, and experimental heating or rehomogenization. Melt inclusions and matrix glass analyzed in the course of this study from a Loihi basalt, an Izu backarc basalt, and two Oregon Cascade basalts depict a variety of potential processes, including assimilation, degassing, re-equilibration, and H diffusion, resulting in a wide range of measured sulfur speciation.

Melt inclusions tend to record a wider range in measured sulfur speciation than is recorded in the matrix glasses, reflecting the numerous processes recorded by the inclusions. Naturally quenched melt inclusions from Loihi (LO-02-02) have a sulfur speciation that is distinctly different from that of the matrix glass. Based on variations in Cl/K_2O ratio, it appears that this difference is the result of assimilation of a seawater derived brine (Kent et al., 1999a,b), and that the inclusions with low Cl/K_2O record an oxidation state of the magma prior to significant assimilation.

Despite the wide range in sulfur speciation, naturally quenched melt inclusions from the Izu backarc basalt (31-7B) and Quartzville basalt in the Cascades (QV04-3B) overlap with those of their respective matrix glasses. Variations in sulfur speciation in the naturally quenched melt inclusions from these samples likely result dominantly from degassing. In contrast to prior work by Gurenko and Schmincke (2000), degassing of sulfur, occurring concurrent with crystallization in the case of QV04-3B, does result in significant changes to the sulfur speciation.

Results of heating experiments demonstrate that inclusion re-equilibration and/or H diffusion may exert significant control over the oxidation state of the melt inclusion. Both processes however will result in the oxidation of the melt. H diffusion, resulting from the dissociation of water, may have greater influence over the oxidation state of the inclusion than re-equilibration, however due to H_2 in the furnace atmosphere, quantitative determination of the effects of H diffusion are not possible in this case. H diffusion and re-equilibration will both promote the formation of sulfide globules, further increasing the S^{6+}/S_{total}.

For samples 31-7B and QV04-3B, inclusions rehomogenized at temperatures near the estimated olivine crystallization temperatures for short durations (<10–15 min), measured sulfur speciation accurately reproduces the ratio of S^{6+}/S_{total} determined from naturally quenched, glassy melt inclusions. In contrast, the Oregon Cascade Cayuse crater basalt (CC02-1) appears to have undergone significant post-entrapment modification, possibly as a result of slow cooling within the lava flow from which is was collected, including re-equilibration and potentially H diffusion. This modification of the melt inclusion composition is reflected in the wide variation of measured sulfur speciation. When used to correct inclusion compositions, the sulfur speciation generates erroneous oxygen fugacities leading to inclusions which appear far out of equilibrium with their host olivines.

Acknowledgments

The authors would like to thank Paul Wallace and John Donovan for their assistance with initial sulfur

speciation measurements and discussion and Frank Tepley for providing electron microprobe time at OSU. Thanks to Tom Sisson for discussing the possible effects of rehomogenization. Detailed comments from reviewers Nicole Metrich and Leonid Danyushevsky greatly improved this manuscript. Support for this study was provided by a Geological Society of America Student Research Grant and a Kleinman Grant through the USGS awarded to Michael Rowe and by National Science Foundation Grant EAR 0440382.

References

Ariskin, A., Frenkel, M., Barmina, G., Nielsen, R., 1993. COMAGMAT: a Fortran program to model magma differentiation processes. Computers and Geosciences 19, 1155–1170.

Anderson, A.T., Wright, T.L., 1972. Phenocrysts and glass inclusions and their bearing on oxidation and mixing of basaltic magmas, Kilauea Volcano, Hawaii. American Mineralogist 57, 188–216.

Asimow, P.D., Ghiorso, M.S., 1998. Algorithmic modifications extending MELTS to calculate subsolidus phase relations. American Mineralogist 83, 1127–1131.

Carmichael, I.S.E., Ghiorso, M.S., 1986. Oxidation-reduction relations in basic magma: a case for homogenous equilibria. Earth and Planetary Science Letters 78, 200–210.

Carmichael, I.S.E., Ghiorso, M.S., 1990. The effect of oxygen fugacity on the redox state of natural liquids and their crystallizing phases. In: Nicholls, J., Russel, J.K. (Eds.), Modern Methods of Igneous Petrology: Understanding Magmatic Processes. Reviews in Mineralogy, vol. 24, pp. 191–212.

Carroll, M.R., Rutherford, M.J., 1988. Sulfur speciation in hydrous experimental glasses of varying oxidation state: results from measured wavelength shifts of sulfur X-rays. American Mineralogist 73, 845–849.

Carroll, M.R., Webster, J.D., 1994. Solubilities of sulfur, noble gases, nitrogen, chlorine, and fluorine in magmas. In: Carroll, M.R., Holloway, J.R. (Eds.), Volatiles in Magmas. Reviews in Mineralogy, vol. 30, pp. 231–279.

Christie, D.M., Carmichael, I.S.E., Langmuir, C.H., 1986. Oxidation states of mid-ocean ridge basalt glasses. Earth and Planetary Science Letters 79, 397–411.

Cottrell, E., Spiegelman, M., Langmuir, C.H., 2002. Consequences of diffusive reequilibration for the interpretation of melt inclusions. Geochemistry, Geophysics, Geosystems 3. doi:10.1029/2001GC000205.

Danyushevsky, L.V., Della-Pasqua, F.N., Sokolov, S., 2000. Re-equilibration of melt inclusions trapped by magnesian olivine phenocrysts from subduction-related magmas: petrological implications. Contributions to Mineralogy and Petrology 138, 68–83.

Danyushevsky, L.V., McNeill, A.W., Sobolev, A., 2002. Experimental and petrological studies of melt inclusions in phenocrysts from mantle-derived magmas: an overview of techniques, advantages and complications. Chemical Geology 183, 5–24.

De Hoog, J.C.M., Hattori, K.H., Hoblitt, R.P., 2004. Oxidized sulfur-rich mafic magma at Mount Pinatubo, Philippines. Contributions to Mineralogy and Petrology 146, 750–761.

Fialin, M., Bezos, A., Wagner, C., Magnein, V., Humler, E., 2004. Quantitative electron microprobe analysis of $Fe^{3+}/\Sigma Fe$: basic concepts and experimental protocol for glasses. American Mineralogist 98, 654–662.

Gerard, O., Jaoul, O., 1989. Oxygen diffusion in San Carlos olivine. Journal of Geophysical Research 94, 4119–4128.

Ghiorso, M.S., Sack, R.O., 1995. Chemical mass transfer in magmatic processes. IV. A revised and internally consistent thermodynamic model for the interpolation and extrapolation of liquid-solid equilibria in magmatic systems at elevated temperatures and pressures. Contributions to Mineralogy and Petrology 119, 197–212.

Gualtieri, A.F., Gemmi, M., Dapiaggi, M., 2003. Phase transformations and reaction kinetics during the temperature induced oxidation of natural olivine. American Mineralogist 88, 1560–1574.

Gurenko, A.A., Schmincke, H-U., 2000. S concentrations and its speciation in Miocene basaltic magmas north and south of Gran Canaria (Canary Islands): constraints from glass inclusions in olivine and clinopyroxene. Geochimica et Cosmochimica Acta 64, 2321–2337.

Hauri, E.H., 2002. SIMS analysis of volatiles in silicate glasses, 2: isotopes and abundances in Hawaiian melt inclusions. Chemical Geology 183, 115–141.

Hedenquist, J.W., Lowenstern, J.B., 1994. The role of magmas in the formation of hydrothermal ore deposits. Nature 370, 519–527.

Hochstaedter, A.G., Gill, J.B., Taylor, B., Ishizuka, O., Yuasa, M., Morita, S., 2000. Across-arc geochemical trends in the Izu-Bonin arc: constraints on source composition and mantle melting. Journal of Geophysical Research 105, 495–512.

Imai, A., Listanco, E.L., Fujii, T., 1993. Petrologic and sulfur isotopic significance of highly oxidized and sulfur-rich magma of Mt. Pinatubo, Philippines. Geology 21, 699–702.

Jugo, P.J., Luth, R.W., Richards, J.P., 2005a. Experimental data on the speciation of sulfur as a function of oxygen fugacity in basaltic melts. Geochimica et Cosmochimica Acta 69, 497–503.

Jugo, P.J., Luth, R.W., Richards, J.P., 2005b. An experimental study of the sulfur content in basaltic melts saturated with immiscible sulfide or sulfate liquids at 1300 °C and 1.0 GPa. Journal of Petrology 46, 783–798.

Kent, A.J.R., Norman, M.D., Hutcheon, I.D., Stolper, E.M., 1999a. Assimilation of seawater-derived components in an oceanic volcano: evidence from matrix glasses and glass inclusions from Loihi seamount, Hawaii. Chemical Geology 156, 299–319.

Kent, A.J.R., Clague, D.A., Honda, M., Stolper, E.M., Hutcheon, I.D., Norman, M.D., 1999b. Widespread assimilation of a seawater-derived component at Loihi Seamount, Hawaii. Geochimica et Cosmochimica Acta 63, 2749–2761.

Luhr, J.F., 1990. Experimental phase relations of water- and sulfur-saturated arc magmas and the 1982 eruptions of El Chichon Volcano. Journal of Petrology 31, 1071–1114.

Massare, D., Metrich, N., Clocchiatti, R., 2002. High-temperature experiments on silicate melt inclusions in olivine at 1 atm: inference on temperatures of homogenization and H_2O concentrations. Chemical Geology 183, 87–98.

Mathez, E.A., 1984. Influence of degassing on oxidation states of basaltic magmas. Nature 310, 371–375.

Matthews, S.J., Moncrieff, D.H.S., Carroll, M.R., 1999. Empirical calibration of the sulphur valence oxygen barometer from natural and experimental glasses: method and applications. Mineralogical Magazine 63, 421–431.

Metrich, N., Schiano, P., Clocchiatti, R., Maury, R.C., 1999. Transfer of sulfur in subduction settings: an example from Bataan Island (Luzon volcanic arc, Philippines). Earth and Planetary Science Letters 167, 1–14.

Metrich, N., Bonnin-Mosbah, M., Susini, J., Menez, B., Galoisy, L., 2002. Presence of sulfite (S^{IV}) in arc magmas: implications for volcanic sulfur emissions. Geophysical Research Letters 29. doi:10.1029/2001GL014607.

Metrich, N., Berry, A., O'Neill, H., Susini, J., 2005. A XANES study of sulfur speciation in synthetic glasses and melt inclusions (abs): Geochimica et Cosmochimica Acta 69 (10) supplement 1, A51.

Nielsen, R.L., Michael, P., Sours-Page, R., 1998. Chemical and physical indicators of compromised melt inclusions. Geochimica et Cosmochimica Acta 62, 831–839.

Paris, E., Giuli, G., Carroll, M.R., 2001. The valence and speciation of sulfur in glasses by X-ray absorption spectroscopy. Canadian Mineralogist 39, 331–339.

Putnis, A., 1979. Electron microscopy and petrography of high temperature oxidation in olivine from Rhum layered intrusion. Mineralogical Magazine 43, 293–296.

Roedder, E., 1979. Origin and significance of magmatic inclusions. Bulletin de Mineralogie 102, 487–510.

Roedder, E., Emslie, R., 1970. Olivine-liquid equilibrium. Contributions to Mineralogy and Petrology 29, 275–289.

Rowe, M.C., 2006. The role of subduction fluids in generating compositionally diverse basalts in the Cascadia subduction zone. PhD thesis, Oregon State University, Corvallis, OR, p. 441.

Rowe, M.C., Nielsen, R.L., Kent, A.J.R., 2006. Anomalously high Fe contents in rehomogenized olivine hosted melt inclusions from oxidized magmas. American Mineralogist 91, 82–91.

Ryerson, F.J., Durham, W.B., Cherniak, D.J., Lanford, W.A., 1989. Oxygen diffusion in olivine: effect of oxygen fugacity and implications for creep. Journal of Geophysical Research 94, 4105–4118.

Sack, R., Carmichael, I., Rivers, M., Ghiorso, M., 1980. Ferric-ferrous equilibria in natural silicate liquids at 1 bar. Contributions to Mineralogy and Petrology 75, 369–376.

Sato, M., Wright, T.L., 1966. Oxygen fugacities directly measured in magmatic gases. Science 153, 1103–1105.

Sobolev, A.V., Chaussidon, M., 1996. H_2O concentrations in primary melts from suprasubduction zones and mid-ocean ridges: Implications for H_2O storage and recycling in the mantle. Earth and Planetary Science Letters 137, 45–55.

Wallace, P.J., 2003. From mantle to atmosphere: magma degassing, explosive eruptions, and volcanic volatile budgets. In: De Vivo, B., Bodnar, R.J. (Eds.), Melt Inclusions in volcanic systems: methods, applications and problems. Developments in Volcanology, vol. 5, pp. 105–127.

Wallace, P.J., 2005. Volatiles in subduction zone magmas: concentrations and fluxes based on melt inclusion and volcanic gas data. Journal of Volcanology and Geothermal Research 140, 217–240.

Wallace, P.J., Carmichael, I.S.E., 1992. Sulfur in basaltic magmas. Geochimica et Cosmochimica Acta 56, 1863–1874.

Wallace, P.J., Carmichael, I.S.E., 1994. S speciation in submarine basaltic glasses as determined by measurements of SKα X-ray wavelength shifts. American Mineralogist 79, 161–167.

Winther, K.T., Watson, E.B., Korenowski, G.M., 1998. Magmatic sulfur compounds and sulfur diffusion in albite melt at 1 GPa and 1300–1500 °C. American Mineralogist 83, 1141–1151.